



ARTICLE

Antibacterial Chitosan-Gelatin Microcapsules Modified with Green-Synthesized Silver Nanoparticles for Food Packaging

Long Li, Yanan Lu, Yu Chen, Jiayi Bian, Li Wang and Li Li*

Engineering Research Center of Food Thermal-Processing Technology, College of Food Science and Technology, Shanghai Ocean University, Shanghai, 201306, China

*Corresponding Author: Li Li. Email: l-li@shou.edu.cn

Received: 15 January 2022 Accepted: 01 March 2022

ABSTRACT

Silver nanoparticles (Ag NPs) are an effective antibacterial agent, but their application in food packaging is limited due to their easy agglomeration and oxidation. In this study, antibacterial microcapsules were fabricated using *Ginkgo biloba* essential oil (GBEO) as core material and chitosan and type B gelatin biopolymer as capsule materials. These antibacterial microcapsules were then modified with green-synthesized Ag NPs, blended into the biopolymer polylactic acid (PLA), and finally formed as films. Physicochemical properties and antibacterial activity against *Escherichia coli* (*E. coli*) and *Staphylococcus aureus* (*S. aureus*) were evaluated. Results showed that the prepared antibacterial PLA films exhibited excellent antibacterial activity against foodborne pathogens. Its TVC exceeded the limit value of 7 log CFU/g at 7 days compared with the 5 days of pure PLA films. Therefore, these films can extend the shelf life of grass carp fillets by 2–3 days under refrigeration.

KEYWORDS

Silver nanoparticles; chitosan; gelatin; microcapsules; antibacterial activity; food packaging

1 Introduction

The silver nanoparticles (Ag NPs) are effective and non-toxic inorganic antibacterial agents [1]. Hence, Ag NPs/polymer composites show potential as food packaging material [2]. Research has been devoted to the green synthesis of Ag NPs by using bio-derived materials as reducing and capping agents to comply with the general principles of green chemistry [3,4]. Plant essential oils can be used as reducing agents and stabilized for green synthesis of nanoparticles, in which Shahram Ahmadi et al. [5] used *Satureja hortensis* essential oil for green-synthesized iron nanoparticles. Among them, *Ginkgo biloba* essential oil (GBEO) can be employed to reduce metal silver ions and thereby synthesize biologically active and stable Ag NPs. During the thermal processing of PLA films, Ag NPs easily agglomerate and oxidized; phytochemicals (such as the flavonoids and terpenoids in GBEO) can prevent this agglomeration by covering the Ag NPs to increase their stability [4].

Microencapsulation is a technology in which a solid, liquid, or gas (core) is wrapped in a continuous polymer material to create microcapsules [6]. Chitosan is a biodegradable, non-toxic, and natural polymer amino polysaccharide [7]. This cationic polymer is derived from chitin and abundantly found in the exoskeletons and shells of crustaceans and fungal cell walls, making it an ideal candidate for



sustained-release capsule materials [8]. Gelatin derived from collagen has good film-forming properties, low cost, biodegradability, and non-toxicity. Therefore, this protein can be selected as an ideal capsule material for encapsulating fat-soluble liquid cores such as essential oils. Chitosan and gelatin can be obtained from the wastes of fishery and meat industries, respectively. Chitosan is the only polysaccharide that is positively charged below pH 6.0, and type B gelatin is negatively charged above the isoelectric point of pH 4.8 [8,9]. Therefore, chitosan can be used as the capsule material of microcapsules through complex coacervation with type B gelatin. The flavonoids and phenolic compounds in GBEO show strong antibacterial and antioxidant capabilities and thus could be used as a core material to prepare sustained-release microcapsules [10–12].

Among biopolymers, polylactic acid (PLA) has excellent biodegradability and biocompatibility, mechanical properties equivalent to petroleum-based polymers (such as polyethylene and polypropylene), high transparency, and good processability [13]. This aliphatic polyester is polymerized by lactic acid monomers. Its monomers are mainly derived from renewable agricultural resources, such as corn, sugar cane, and sugar beets [14]. Owing to its biodegradability and biocompatibility, PLA has been highly recognized and applied in the fields of biomedicine, agriculture, and packaging. The U.S. Food and Drug Administration approved this material as “Generally Recognized as Safe” [15].

In this work, antibacterial microcapsules were prepared through complex coacervation and spray drying by using GBEO as core material and chitosan and type B gelatin polymer as capsule materials. The chitosan-gelatin microcapsules were modified with green-synthesized Ag NPs and added to degradable PLA films, which were then applied to preserve grass carp (*Ctenopharyngodon idellus*) fillets. This work aims to prepare a food packaging composite material with antibacterial, non-toxic, and degradable properties by using an environmentally friendly method (Fig. 1).

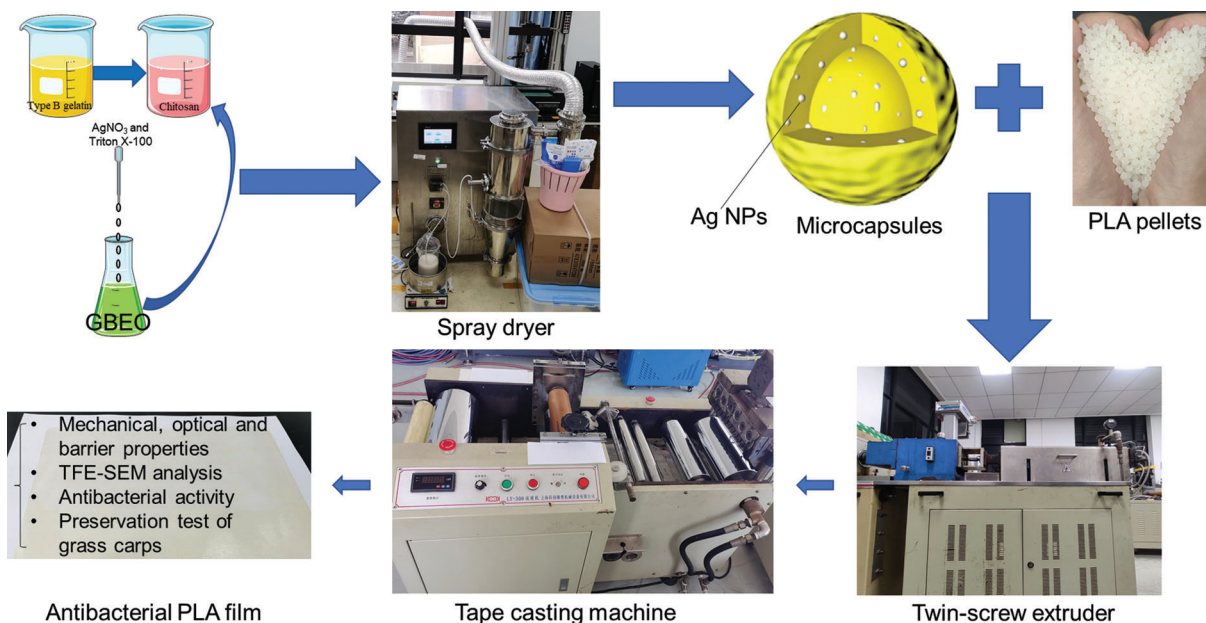


Figure 1: Schematic representation

2 Materials and Methods

2.1 Materials

For microcapsules production, chitosan acquired from Aladdin (CAS 9012-76-4, degree of deacetylation $\geq 95\%$, viscosity: 100–200 mpa.s, Shanghai, China) and type B gelatin purchased from Sinopharm (CAS 9000-70-8, Shanghai, China) were used as a biopolymer capsule materials. Silver nitrate obtained from Sinopharm (AgNO_3 , CAS 7761-88-8, Shanghai, China), the *Ginkgo biloba* essential oil (GBEO, distillation, 99%) purchased from Ji'an Zhongxiang Natural Plant Co., Ltd. (Ji'an, China), and polyethylene glycol octyl phenyl ether (Triton X-100, CAS 9002-93-1) from Shanghai Lingfeng Chemical Reagent Co., Ltd., China were employed as core materials. Acetic acid (CAS 64-19-7, $\geq 99.7\%$, Shanghai, China) was purchased from Aladdin. Sodium hydroxide (NaOH , CAS 1310-73-2, Shanghai, China) was used to adjust pH.

For PLA films production, PLA (LX575) produced by Total Corbion was purchased from Shanghai Shengxiang International Trading Co., Ltd., China.

Pathogens, such as *Escherichia coli* (*E. coli*, ATCC 35218) and *Staphylococcus aureus* (*S. aureus*, ATCC 25913) were acquired from laboratory-preserved strains. Trypticase soy broth and plate count agar (PCA) were obtained from Beijing Land Bridge Technology Co., Ltd. (Beijing, China). Ethanol (A.R., CAS 64-17-5, $\geq 99.7\%$, Shanghai, China) was purchased from GENERAL-REAGENT. Water was purified by a Milli-Q Plus purification system (Millipore, Shanghai, China). Fresh cultured grass carps with the average weight of 4.0 ± 0.5 kg were purchased from GuZong Road Market (Shanghai, China).

2.2 Preparation of Microcapsules

2.2.1 Preparation of Capsule Material

Chitosan solution (0.5% w/v) was prepared through the electromagnetic stirring (DF-101S, Shanghai Lichen-BX Instrument, Shanghai, China) of a chitosan suspension in 1% (v/v) acetic acid solution at room temperature for 145 min. Type B gelatin solution (0.5% w/v) was prepared by swelling with water for 130 min and then magnetically stirring at 60°C for 10 min. The mass ratio of chitosan to type B gelatin was 1:1. The mixture was stirred for 60 min, adjusted to pH 5.5 with NaOH solution by a laboratory pH meter (PHSJ-4F, LEICI, China), and then stirred again for 80 min.

2.2.2 Green Synthesis of Core Material

In brief, 0.1 mol/L AgNO_3 solution, GBEO, and surfactant Triton X-100 with volume ratio of 20:10:1 were used as core materials for the microcapsules and then magnetically stirred in the dark at 70°C to form Ag NPs through silver ion bio-reduction.

The following microcapsules were prepared: A: replacing 0.1 mol/L AgNO_3 solution and GBEO with water as the core material; B: with water instead of 0.1 mol/L AgNO_3 solution as the core material; and C: with 0.1 mol/L AgNO_3 solution and GBEO as the core material. As shown in [Table 1](#):

Table 1: The content of microcapsules

	Chitosan solution	Type B gelatin solution	GBEO	AgNO_3 solution	Triton X-100
Microcapsules A	√	√			√
Microcapsules B	√	√	√		√
Microcapsules C	√	√	√	√	√

2.2.3 Characterizations of Green-Synthesized Ag NPs

The Fourier transform infrared spectroscopy (FTIR) images of the Ag NPs were obtained from 400 cm^{-1} to 4000 cm^{-1} by using a FTIR-650 (Tianjin, China) [16]. UV-visible spectrophotometry was conducted from 300 nm to 650 nm using a U-3900 (Hitachi, Japan) spectrophotometer. Photoluminescence was evaluated by using a F-7100 fluorescence spectrophotometer (Hitachi, Japan), and 280 nm excitation wavelength was selected to study the fluorescence characteristic of Ag NPs [17]. Morphology was analyzed using a HT7800 transmission electron microscope (TEM, Hitachi, Japan). Particle size was calculated on the basic TEM images by an image analysis software (Image J, NIH, USA) [18]. The Ag element of the Ag NPs was detected via X-ray photoelectron spectroscopy (XPS, Thermo Fisher Scientific, Escalab 250Xi).

2.2.4 Preparation of Microcapsules through Spray Drying

The core materials in “2.2.2” were added dropwise to the capsule material solution in “2.2.1”, magnetically stirred for 30 min, and homogenized at 10,000 rpm for 20 min (IKA T25 digital ULTRA-TURRAX, German) to form oil-in-water (O/W) emulsion. The ratio of capsule materials, 0.1 mol/L AgNO_3 solution, GBEO, and surfactant Triton X-100 was 5:20:10:1 (w/v/v/v). Spray drying of emulsions was conducted using a low-temperature spray dryer (YC-1800, Shanghai, China) at $120^\circ\text{C}/75^\circ\text{C}$ inlet/outlet temperature and feeding speed of 17 rpm inside a laboratory.

2.3 Characterizations of Microcapsules

The FTIR spectra of the samples were obtained between 400 and 4000 cm^{-1} . The microscopic morphology of microcapsules was examined using a SU5000 thermal field emission scanning electron microscope (TFE-SEM, Hitachi, Japan) [7]. Particle size was calculated on the basic TFE-SEM images. Energy dispersive X-ray spectrometer (EDS) attached to the desktop scanning electron microscope (Phenom XL, Phenom-World BV, Eindhoven, Netherlands) at an accelerating voltage of 15 keV was employed for the qualitative and quantitative analysis of elements in microcapsules C containing Ag element [19]. XPS was used to detect the Ag element of the microcapsules C modified with Ag NPs [20].

2.4 Preparation of Antibacterial PLA Films

The antibacterial PLA films were prepared using the melt blending method of Jiang et al. [21] with some modifications. Films with an average thickness of $50 \pm 3\ \mu\text{m}$ were prepared through extrusion-casting. The PLA pellets were dried in a 75°C oven for 3 h and then blended with the microcapsules. The mixture was extruded through a twin-screw extruder (Kechuang Equipment Co., Ltd., Shanghai, China) to obtain PLA/microcapsules pellets. The temperature of each stage was 140°C – 145°C – 150°C – 155°C – 160°C – 155°C – 150°C (from the inlet to the outlet) with a screw speed of 90 rpm. Finally, the PLA/microcapsules pellets were casted into films by using a tape casting machine (Kechuang Equipment Co., Ltd., Shanghai, China). The temperature was 100°C – 150°C – 155°C – 160°C – 165°C – 165°C – 165°C (from the inlet to the outlet) with a screw speed of 90 rpm. Table 2 shows the content of films.

Table 2: The content of films

	PLA	2 wt.% microcapsules A	2 wt.% microcapsules B	2 wt.% microcapsules C
Control films	100 wt.%			
PLA-A	98 wt.%	√		
PLA-B	98 wt.%		√	
PLA-C	98 wt.%			√

2.5 Characterizations of PLA Films

The thickness of the PLA films was determined with a spiral micrometer (Nanjing NSCING Measuring Instrument Co., Ltd., China) in accordance with GB/T20919-2007. The tensile strength (TS) and elongation at break (EAB) of the films (12 cm × 1.5 cm) were measured at 25°C by a XLW (EC)-1502 auto tensile tester (Labthink Instrument Co., Ltd., Jinan, China) in accordance with ASTM D882-12(2012). Stretching speed was set to 50 mm/min. Optical properties, including the transmittance (T) and haze (H) of the films, were measured with a WGT/S haze and transmittance testing machine (Shanghai Precision Instrument Co., Shanghai, China) in accordance with ASTM D1003-00(2000) [22].

The water vapor permeability (WVP) of films was determined at 38°C and 10% RH with a Water Vapor Transmission Rate Tester (W-B-31E, Labstone, Guangzhou, China) in accordance with GB/T 1037.

The microscopic morphology of films was examined using a TFE-SEM. The films were freeze-fractured in liquid nitrogen and sputter-coated with gold and platinum powder to observe their cross-sectional morphology at an electron beam voltage of 10 KV [21].

The antibacterial activity of films against *E. coli* and *S. aureus* was studied. Sterilized 500 mg film discs (6 mm diameter) were placed in 20 mL of *E. coli* (gram-negative) and *S. aureus* (gram-positive) suspensions (10^5 CFU/mL) and shook at 200 rpm for 24 h in a 37°C incubator shaker. The film discs containing the bacterial suspensions were placed in a 24-well plate and washed twice with 2 mL of 0.1 mol/L phosphate buffered saline (PBS) solution. The samples were fixed with 2 mL of 2.5% (v/v) glutaraldehyde for 4 h at 4°C. After the samples were washed twice with 2 mL 0.1 mol/L PBS solution again, 2 mL of 50%, 70%, 80%, 90%, and 100% (v/v) ethanol were used for stepwise dehydration (10 min per step). After drying at 37°C overnight, the samples were sputter-coated with gold for 3 min prior to TFE-SEM.

2.6 Preservation Test of Grass Carps

On June 2021, cultured grass carps were purchased and transported to the laboratory alive in clean water with oxygenation within 2 h. In the laboratory, the grass carps were percussively stunned by a blow of sufficient strength to the head. The fish were then killed by immediately sectioning the spinal cord at the base of the head to meet the requirements of ethical standards [23]. The guts, skin, and bones of grass carps were removed, and the fish were washed with sterile normal saline solution and sliced into similar weight (50 ± 3 g). All fish experiments were performed in strict accordance with the European Food Safety Authority (2009) and EU Directive 2010/63/EU. The slices were wrapped in kitchen paper to dry the excess water on the surface and then packaged with four types of films: control films (control), PLA-A (A), PLA-B (B) and PLA-C (C). The packages (internal size: 15 cm × 15 cm, thickness: 50 ± 3 μm) were then sealed with a hand pressure sealing machine (YNL-200, DUOXI, China). All samples were immediately stored in a refrigerator at 4 ± 0.5 °C for subsequent evaluations. Three random samples of white dorsal muscle were taken from each group for analysis, and the sampling times were 0, 2, 4, 6, 8, and 10 days of storage.

Control: packaged with control films

A: packaged with PLA-A

B: packaged with PLA-B

C: packaged with PLA-C

2.6.1 Total Volatile Basic Nitrogen (TVB-N)

TVB-N was measured using a Kjeltac 8400 (FOSS, Denmark). In brief, 10 g of grass carp sample was distilled with 1 g of magnesium oxide. The distillate was collected in 1% boric acid solution in the presence

of indicators (methyl red mixed with bromocresol green) and then titrated with 0.1 mol/L HCl standard solution. TVB-N was expressed as milligram nitrogen per 100 g of grass carp sample (mgN/100 g) [24].

2.6.2 Total Viable Counts (TVC)

Grass carp specimens were minced under sterile conditions. A portion of the samples (5 g) was diluted with 45 mL of sterile 0.85% normal saline and homogenously slapped for 3 min using a HX-4 beating sterile homogenizer (Shanghai Huxi Industrial Co., Ltd., China). Tenfold serial dilution of the homogenized mixture was prepared with normal saline, pipetted (1 mL), and mixed with PCA medium (incubated at $30 \pm 0.5^\circ\text{C}$ for 72 h). All counts were expressed as logarithms of the number of colony forming units per gram (log CFU/g), and each experiment was performed in triplicate [25].

2.7 Statistical Analysis

All measurements were conducted in triplicate, and the data were statistically analyzed using SPSS Statistics 26. Comparisons among samples were performed using one-way ANOVA, and statistically significant difference was defined at $p < 0.05$.

3 Results and Discussion

3.1 Analysis of Green-Synthesized Ag NPs

FTIR measurement was conducted on the green-synthesized Ag NPs to identify the functional groups of their active components. The following characteristic peaks were observed: 3484 (O-H stretching), 2930 (C-H stretching), 2857 (C-H stretching), 1749 (C=O stretching), and 1099 cm^{-1} (C-O stretching) (Fig. 2a). These findings revealed the presence of phenolic, flavonoids, and other molecules in GBEO, which may be beneficial to the bio-reduction of silver ions to Ag NPs. FTIR spectra also confirmed that the phytochemicals from GBEO have dual functions of reducing and stabilizing Ag NPs.

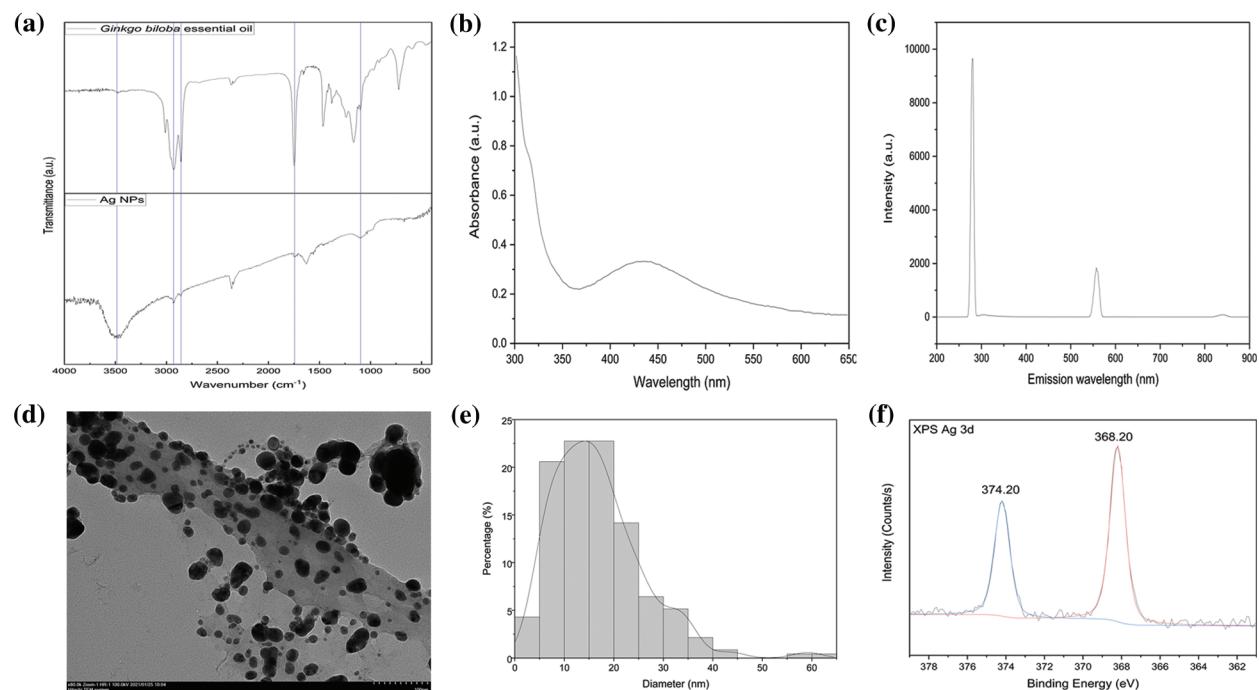


Figure 2: (a) Fourier transform infrared spectroscopy spectra of *Ginkgo biloba* essential oil and silver nanoparticles (Ag NPs). (b) UV-visible absorbance study of Ag NPs. (c) Fluorescence spectrum of Ag NPs formed with excitation at 280 nm. (d) Transmission electron microscope image of Ag NPs. (e) Size distribution of Ag NPs. (f) X-ray photoelectron spectroscopy spectra of Ag NPs

The addition of GBEO to AgNO_3 solution resulted in color change from green to brown due to Ag NP production. This color change can be attributed to the excitation of surface plasmon vibrations in Ag NPs [26]. The UV-vis spectrum of biogenic synthesized Ag NPs is shown in Fig. 2b. The surface plasmon resonance (SPR) of Ag NPs produced a peak centered near 436 nm [17], implying the transformation of Ag^+ into Ag^0 . According to Mie's theory, small spherical or quasi-spherical nanocrystals should exhibit a single SPR band [27]. The UV-vis spectrum is a characteristic absorption peak that is correlated with the localized SPR of spherical Ag NPs [28].

Ag NPs exhibit visible photoluminescence. The room-temperature fluorescence spectrum of the prepared Ag NPs excited at 280 nm is shown in Fig. 2c. The Ag NPs were found to be luminescent with two emissions at 280 and 557 nm upon excitation at 280 nm. The luminescence at 280 nm can be attributed to presence of the phytochemicals from GBEO. The characteristics of the emission spectrum were similar to those in previous reports [17], thus confirming the successful preparation of Ag NPs.

TEM was used to characterize the surface morphologies and particle size of synthesized Ag NPs. The Ag NPs showed a typical spherical and ellipsoidal morphology. Some exhibited irregular structures and slight aggregation (Fig. 2d) due to insufficient dispersion in ethanol during sample preparation. The average particle size measured from the TEM images was around 17 nm (Fig. 2e). These results conformed to the shape of SPR band in the UV-vis spectrum.

Fig. 2f shows the typical XPS spectra of Ag NPs, which were basically double-peaked, namely, $3d_{5/2}$ and $3d_{3/2}$. The XPS Ag 3d spectra of this sample showed two individual peaks at 368.20 and 374.20 eV with a spin-orbit separation of 6 eV [29,30], keeping the ratio of those signals as 3:2 [31], respectively. This finding indicated that the metallic silver was successfully synthesized.

3.2 Analysis of Microcapsules

3.2.1 FTIR Analysis

The main composition of raw materials and different microcapsules can be deduced from FTIR analysis (Fig. 3). The characteristic peaks observed in the range of $3200\text{--}3500\text{ cm}^{-1}$ were attributed to the stretching vibration of O-H and N-H [32]. The spectrum of GBEO displayed a characteristic peak around 1749 cm^{-1} (C=O stretching), which confirmed the presence of flavonoids, the main bioactive compounds in GBEO. The major characteristic peaks associated with chitosan powder were observed at 1655 cm^{-1} (C=O stretching, amide I), 1600 cm^{-1} (N-H bending, amide II), 1425 cm^{-1} (N-H stretching, amide II), 1383 cm^{-1} (N-H stretching, amide III), and 896 cm^{-1} (pyranose ring) [33]. The spectrum for type B gelatin showed amide I peak (C=O stretching) at 1649 cm^{-1} , amide II peak (N-H bond and C-H stretching) at 1535 cm^{-1} , and amide III peak (C-N stretching plus N-H bending) at 1234 cm^{-1} [34]. The spectra of microcapsules A-C were considerably different than pure chitosan and type B gelatin indicating that some changes occurred in the function groups of the microcapsules. The spectra of microcapsules A-C at 1579 cm^{-1} represented the interaction of amide II band to form Schiff base and can be attributed to N-H bending and C-N stretching vibration. The amide II spectrum originated mainly from the axial stretching of coupling C-N stretching and the angular deformation of N-H bending [34]. A strong absorption peak of C-N stretching vibration was also found at 1414 cm^{-1} compared with that of pure, raw chitosan and type B gelatin. These results indicated an interaction between chitosan and type B gelatin. The spectra of GBEO, microcapsules B, and C showed characteristic absorption peaks at 1749 cm^{-1} (C=O stretching) and 723 cm^{-1} (O-H out-of-plane bending). In addition, compared with the spectrum of microcapsules A, the positions of the main peaks of microcapsules B and C did not change. This finding indicated the lack of interaction between GBEO and chitosan-gelatin capsule materials and the existence of GBEO in microcapsules B and C.

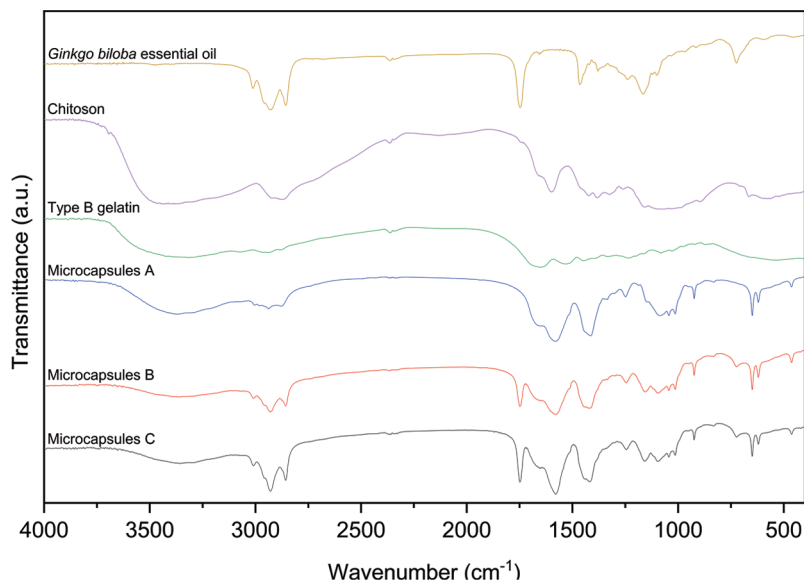


Figure 3: Fourier transform infrared spectroscopy spectra of different microcapsules and main raw materials

3.2.2 TFE-SEM Analysis

Fig. 4 shows the surface morphologies and particle size of microcapsules. Microcapsules A showed an irregular appearance and uneven size distribution due to solvent evaporation during spray drying (Fig. 4a). With GBEO addition, the surface of microcapsules B in Fig. 4b became smoother than that of microcapsules A, suggesting that GBEO improved the structural resistance. Microcapsules C (Fig. 4c) exhibited a partially wrinkled and porous structure that can be attributed to the presence of Ag NPs. Moreover, the average sizes of microcapsules A, B and C were approximately 1.75, 2.17, and 2.25 μm , respectively, as shown in Figs. 4d–4f, respectively.

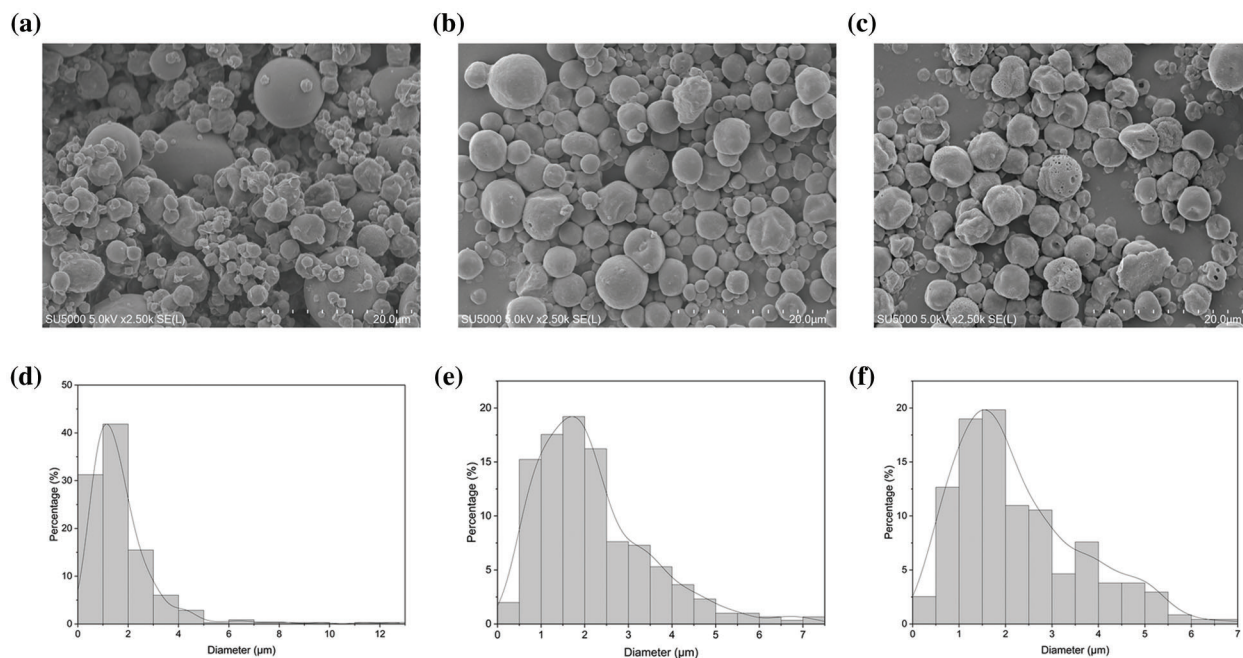


Figure 4: Thermal field emission scanning electron microscope micrographs of (a) microcapsules A, (b) microcapsules B, and (c) microcapsules C. Particle size distribution of (d) microcapsules A, (e) microcapsules B, and (f) microcapsules C

3.2.3 EDS and XPS Analysis

The presence of Ag NPs in microcapsules C was confirmed in the inset of Fig. 5. The optical absorption peaks were observed around 3 keV, which is typical for Ag nanocrystallite absorption due to SPR. EDS spectroscopy also showed a strong peak around 0.2 keV, which is similar to a previous report [35]. The Ag NPs were evenly distributed throughout the microcapsules, and their proportion was approximately 1.33 wt.%. This value corresponded to the feed ratio. Carbon, oxygen, nitrogen, and sodium were also observed. These elements are the main chemical components of microcapsules C because the penetration of the high-energy electron beams is up to 1 μm depth. These results indicated that the Ag NPs may be evenly distributed throughout the microcapsules including in the capsule and core.

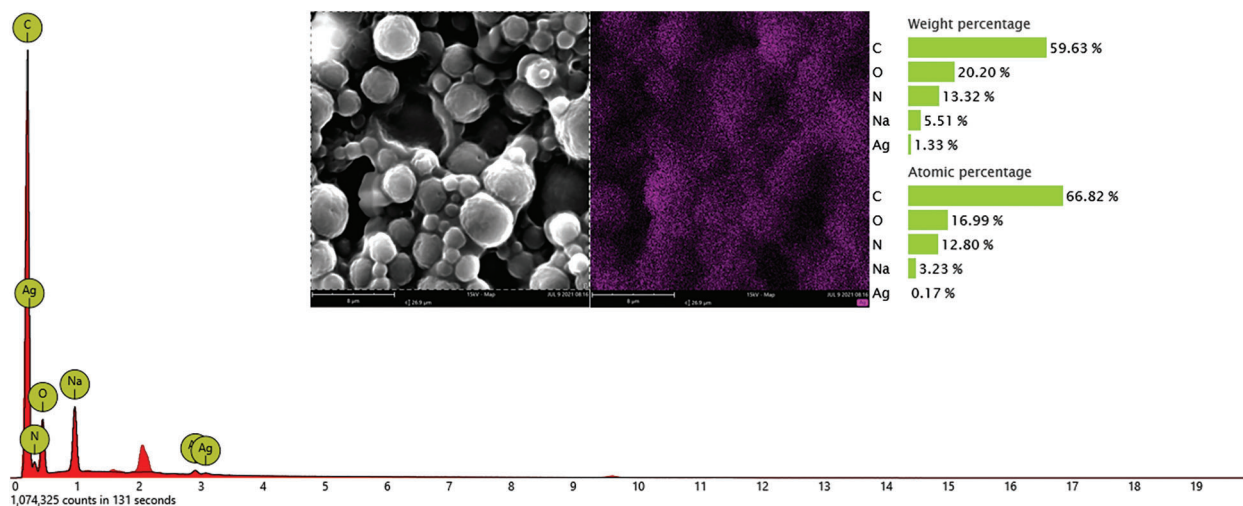


Figure 5: Energy dispersive X-ray spectrometer spectrum of microcapsules C

XPS survey was conducted on the samples to analyze the binding energy of Ag NPs in microcapsules C. As shown in the high-resolution XPS spectra in Fig. 6, the Ag 3d region underwent spin-orbital splitting and appeared at 368.40 and 374.40 eV, which classified the nanoparticles as metallic silver [36].

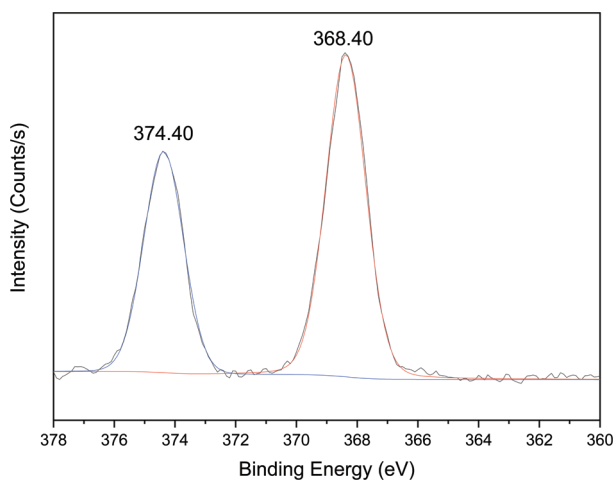


Figure 6: High-resolution X-ray photoelectron spectroscopy spectra of microcapsules C for the silver element

3.3 Analysis of PLA Films

3.3.1 Physicochemical Properties of PLA Films

Table 3 shows the mechanical and optical properties of PLA films. The addition of microcapsules A, B, and C (PLA-A, B, and C, respectively) reduced the tensile properties of the PLA films. This phenomenon can be attributed to the interfacial adhesion between the microcapsules and the PLA resin matrix that produced small holes and cracks in the film structure. Compared with the control films, PLA-A, B, and C had significantly reduced T values ($p < 0.05$) but significantly increased H values ($p < 0.05$), indicating that the added microcapsules reduced the transparency of the PLA films.

Table 3: Mechanical, optical, and barrier properties of different PLA films

	Control films	PLA-A	PLA-B	PLA-C
Thickness (μm)	50.33 ± 2.08^a	50.67 ± 1.53^a	51.00 ± 2.65^a	52.33 ± 2.89^a
Horizontal TS (Mpa)	42.21 ± 0.93^d	18.12 ± 0.79^a	20.82 ± 0.79^b	22.14 ± 0.55^c
Horizontal EAB (%)	3.10 ± 0.32^b	1.43 ± 0.15^a	1.46 ± 0.23^a	1.40 ± 0.10^a
Longitudinal TS (Mpa)	80.41 ± 1.24^c	26.08 ± 1.47^a	29.44 ± 1.66^b	31.74 ± 1.57^b
Longitudinal EAB (%)	4.75 ± 0.39^b	3.10 ± 0.55^a	2.50 ± 0.61^a	2.70 ± 0.17^a
T (%)	86.34 ± 0.13^d	75.66 ± 0.29^c	74.06 ± 0.15^b	73.66 ± 0.11^a
H (%)	4.91 ± 0.50^a	23.85 ± 0.38^b	24.33 ± 0.17^c	25.50 ± 0.18^d
WVP/[$\text{g}/\text{m}^2 \cdot 24 \text{ h}$]	165.45 ± 5.54^a	206.98 ± 3.87^d	174.53 ± 3.40^b	194.75 ± 2.17^c
WVP coefficient/[$10^{-13} \text{ g} \cdot \text{cm}/\text{cm}^2 \cdot \text{s} \cdot \text{Pa}$]	1.61 ± 0.05^a	2.01 ± 0.04^d	1.70 ± 0.03^b	1.91 ± 0.01^c

Note: Data are presented as means \pm standard deviation ($n = 5$). Significant difference ($p < 0.05$) among the values within the same row indicated by different superscripts (a–d) (Control films: 100 wt.% PLA; PLA-A: 98 wt.% PLA + 2 wt.% microcapsules A; PLA-B: 98 wt.% PLA + 2 wt.% microcapsules B; PLA-C: 98 wt.% PLA + 2 wt.% microcapsules C).

Table 3 also presents the barrier properties of the PLA films. The films with microcapsules significantly improved WVP because the hydrophilic groups in the microcapsules allowed the water molecules to be adsorbed on the films, thus facilitating water passage. The pores and cracks formed between the microcapsules and the PLA matrix facilitated the flow of water vapor in the films. In addition, the WVP of PLA-A, B, and C was in the order PLA-A < C < B. The reduction in the resistance of films to water vapor transmission was related to the presence of keto carbonyl and hydroxy groups in GBEO. These components decreased the hydrophobic properties and increased the free volume of the films [22]. Finally, the Ag NPs in microcapsules C also affected the performance of the PLA films to a certain extent.

3.3.2 TFE-SEM Analysis of PLA Films

Fig. 7 shows the cross-sectional microstructure of different PLA films. The internal dispersion of the microcapsules added to the PLA matrix can be directly observed. The cross-section of the control films made of pure PLA resin was mainly smooth, flat, and compact (Fig. 7a). With the microcapsules A addition, PLA-A developed cracks and pores, resulting in a lower compatibility (Fig. 7b). Microcapsules B and C (both contained GBEO) were added to PLA-B and C, respectively (Figs. 7c and 7d). Although these films had some pores, their compatibility and stable dispersion system were better than PLA-A. In addition, the cracks and pores could explain the decreases in TS and EAB compared with the control films (Table 3).

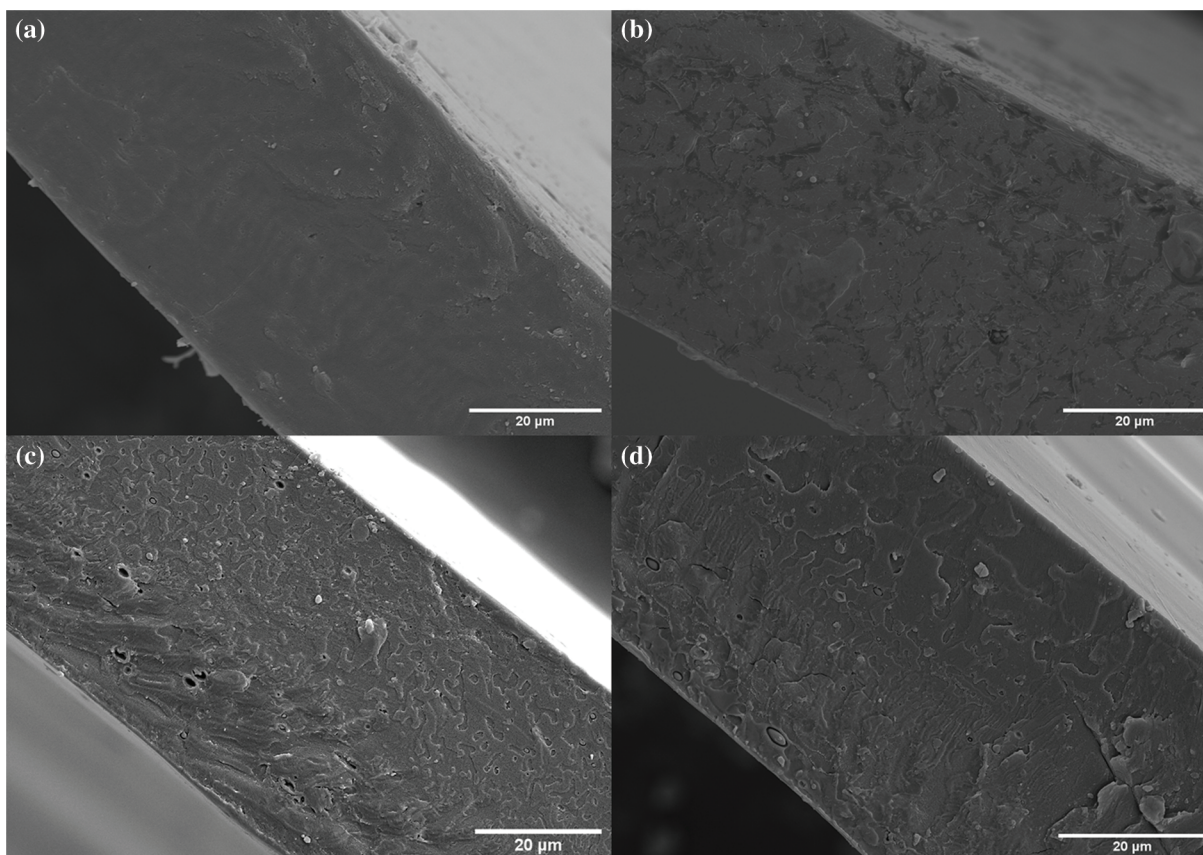


Figure 7: Thermal field emission scanning electron microscope micrographs of (a) control films, (b) PLA-A, (c) PLA-B, and (d) PLA-C

3.3.3 Antibacterial Activity of PLA Films

Fig. 8 shows the TFE-SEM images of *E. coli* treated with different PLA films. As illustrated in Fig. 8a, the *E. coli* cells treated with control films presented a rod-shaped structure and smooth and intact cells. Therefore, the control films basically had no killing effect on *E. coli*. In the *E. coli* cells treated with PLA-A, the cell morphology was slightly deformed with minimal leakage of cell contents (Fig. 8b). After PLA-B treatment, many protoplasts could be seen spreading out on the surface of the bacteria (Fig. 8c). As shown in Fig. 8d, PLA-C had the greatest impact on the bacteria. The cracks formed on the bacterial surface caused a large amount of cell content to flow out. Fig. 8 also displays that the treatment results of *S. aureus* cells showed a similar trend. The results of morphological changes for *S. aureus* were consistent with those for *E. coli* (Figs. 8e–8h).

The $-NH_2$ of chitosan was protonated to $-NH_3^+$, and cationic formation subsequently occurred on its molecular side chain in acetic acid solution (1% v/v). Hence, electrostatic interactions easily occurred between chitosan's positively charged groups and negatively charged bacterial surface. The result is the formation of a bridge that could cause cell wall disruption and intracellular component leakage [37]. The antibacterial mechanism of PLA-C containing microcapsules C (chitosan-gelatin microcapsules modified with Ag NPs) might involve the slow release of silver ions. The discussion of the antibacterial effect of Ag NPs/polymer composites has been reported [38]. After interacting with the surface of bacterial cells through electrostatic attraction, the Ag NPs effectively disrupted important cellular processes, including the release of silver ions, which cause protein deformation, and DNA degradation, in which the silver

ions interact with DNA and nucleotides through its nucleoside moieties [39]. One of the important antibacterial mechanisms of chitosan in PLA-C is to enhance the permeability of bacterial cells. Hence, the interaction between chitosan-gelatin microcapsules and Ag NPs should be synergistic rather than simply additive [40].

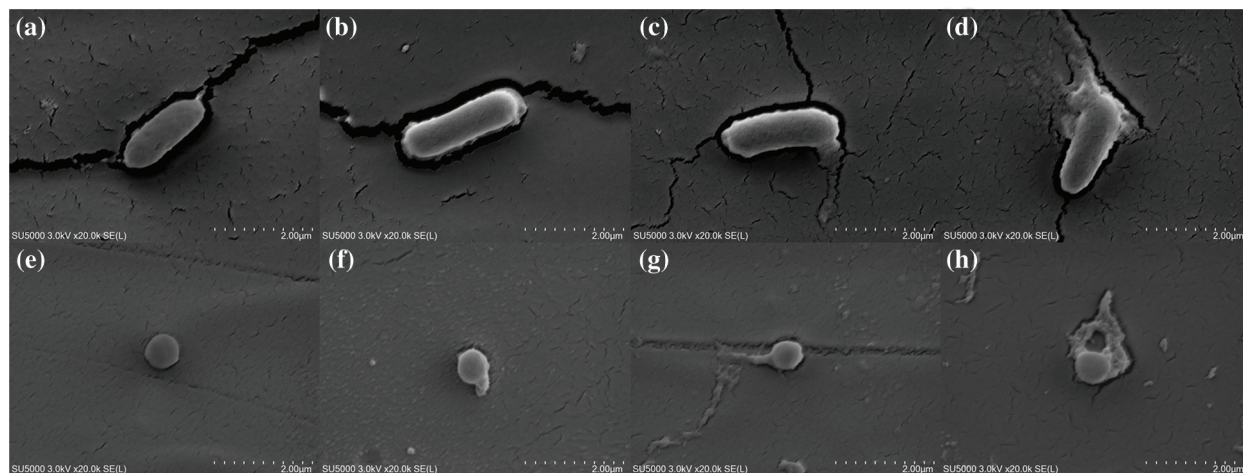


Figure 8: Thermal field emission scanning electron microscope (TFE-SEM) images of *E. coli* treated with (a) control films, (b) PLA-A, (c) PLA-B, and (d) PLA-C. TFE-SEM images of *S. aureus* treated with (e) control films, (f) PLA-A, (g) PLA-B, and (h) PLA-C

3.4 Preservation Test of Grass Carps

3.4.1 TVB-N

TVB-N is one of the important indexes to describe the quality of aquatic products. This term quantifies the presence of volatile alkaline nitrogen, including ammonia, amines, and other alkaline nitrogen-containing compounds, which are formed due to the degradation of protein and non-protein nitrogenous compounds caused by bacteria and endogenous enzymes [41]. A high TVB-N indicates severe fish spoilage, which is not acceptable to people.

As depicted in Fig. 9, all groups exhibited increased TVB-N values with prolonged storage time. The initial TVB-N value of fresh grass carp fillets was approximately 10.91 mgN/100 g. Prior to the 6th day of storage, the increase in TVB-N values for all samples was less evident, especially for experimental group C ($p > 0.05$). Afterward, the TVB-N value of samples packaged with PLA-C was significantly lower than that of other groups during 6–10 days of storage ($p < 0.05$). These results suggested that PLA-C suppressed the increase in TVB-N values and can be used to maintain the freshness of grass carp fillets.

3.4.2 TVC

Microbial spoilage is a common spoilage types of fish, and TVC is an important index to evaluate the shelf life and quality of aquatic products. Fig. 10 shows the changes in the TVC of grass carp fillets. The initial TVC of fresh samples was nearly 3.42 log CFU/g, which was close to the value (3.50 log CFU/g) reported by Zhang et al. [42] for refrigerated fresh grass carp fillets. A low initial TVC value reflects the high quality of fillets and processing hygiene. Afterward, the TVC of all four groups increased with storage time at different rates due to the growth of specific spoilage microorganisms in aquatic products [43]. ICMSF enforced a TVC of 7.0 log CFU/g as the upper acceptability limit for freshwater species. The control group and group A reached the upper tolerable limit after 5.42 and 5.57 days, respectively.

However, groups B and C did not exceed this count at 6 days with values of 6.70 and 5.25 log CFU/g, respectively. The TVC of group C was significantly lower than that of group B ($p < 0.05$). Moreover, group C exceeded the limit at 7.69 days. Compared with the control group (pure PLA films), PLA-C containing chitosan-gelatin microcapsules modified with Ag NPs could prolong the microbiological shelf life of grass carp fillets by 2–3 days.

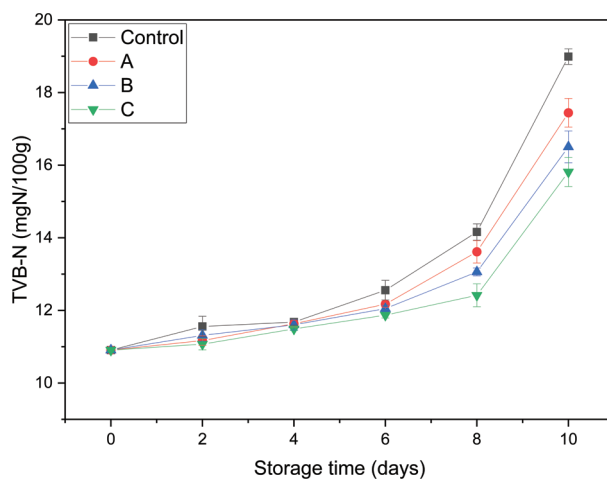


Figure 9: Total volatile basic nitrogen of grass carp fillets packaged with different PLA films (Control: packaged with control films; A: packaged with PLA-A; B: packaged with PLA-B; C: packaged with PLA-C)

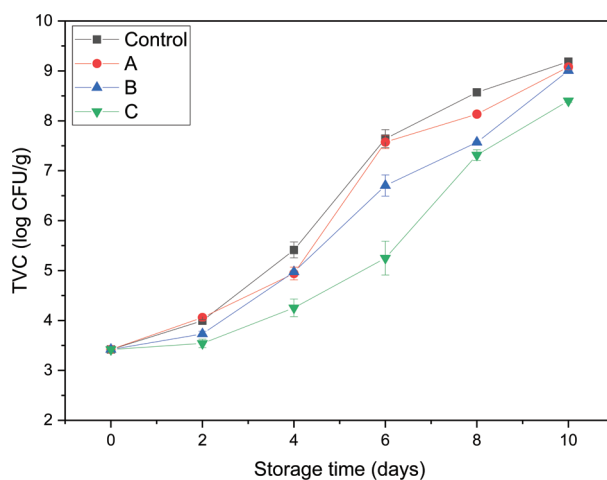


Figure 10: Total viable counts of grass carp fillets packaged with different PLA films (Control: packaged with control films; A: packaged with PLA-A; B: packaged with PLA-B; C: packaged with PLA-C)

4 Conclusions

In this study, antibacterial chitosan-gelatin microcapsules modified with green-synthesized Ag NPs were successfully synthesized and applied to food preservation packaging. First, chitosan-gelatin microcapsules modified with green-synthesized Ag NPs were prepared in compliance with the general principles of green chemistry. The Ag NPs were characterized with TEM, particle size analysis, and XPS and revealed

a typical spherical with an average size of 17 nm. FTIR, TFE-SEM, EDS, and XPS confirmed the successful fabrication of chitosan-gelatin microcapsules modified with Ag NPs. The antibacterial microcapsules were incorporated into biopolymer PLA to form films through extrusion–casting. The prepared material exhibited antibacterial activity against *E. coli* and *S. aureus*. The antibacterial PLA films were then used to preserve grass carp fillets to extend their shelf life, and the results confirmed their antibacterial activity on food. Therefore, the antibacterial chitosan-gelatin microcapsules modified with green-synthesized Ag NPs with good dispersibility and the PLA pellets show potential as a functional and sustainable food preservation packaging material through extrusion–casting.

Authors Contributions: Conceptualization: Long Li, Li Wang, Li Li; Methodology: Long Li, Yanan Lu, Yu Chen, Jiayi Bian; Writing-original draft preparation: Long Li; Writing-review and editing: Long Li, Li Li; Funding acquisition: Li Li; Resources: Li Wang, Li Li; Supervision: Li Li.

Availability of Data and Materials: The datasets used or analysed during the current study are available from the corresponding author on reasonable request.

Acknowledgement: The authors appreciate the assistance provided by the relevant personnel of College of Food Science and Technology of Shanghai Ocean University to the smooth progress of the experiment. The authors are especially grateful to teacher Shaomei Cao of Shanghai University for the technical support in energy dispersive X-ray spectrometer.

Funding Statement: This work was supported by the National Key R&D Program of China (Grant No. 2020YFD0900905).

Conflicts of Interest: The authors declare that they have no conflicts of interest to report regarding the present study.

References

1. Amarasinghe, D., Samarasekara, A., Madhuwanthi, W., Dammage, D. (2018). Nano-silver impregnated wrapping film to keep fruit fresh. *2018 Moratuwa Engineering Research Conference (MERCon)*, pp. 511–516. Katubedda, Sri Lanka.
2. Echegoyen, Y. (2015). *Nano-developments for food packaging and labeling applications*. Germany: Springer International Publishing.
3. Saravanakumara, K., Hua, X. W., Chelliahb, R., Ohb, D. H., Kathiresanc, K. et al. (2020). Biogenic silver nanoparticles-polyvinylpyrrolidone based glycosomes coating to expand the shelf life of fresh-cut bell pepper (*Capsicum annuum* L. var. *grossum* (L.) Sendt). *Postharvest Biology and Technology*, 160, 111039. DOI 10.1016/j.postharvbio.2019.111039.
4. Cheng, J., Lin, X. T., Wu, X. L., Liu, Q., Wan, S. M. et al. (2021). Preparation of a multifunctional silver nanoparticles polylactic acid food packaging film using mango peel extract. *International Journal of Biological Macromolecules*, 188, 678–688. DOI 10.1016/j.ijbiomac.2021.07.161.
5. Ahmadi, S., Fazilati, M., Nazem, H., Mousavi, S. M. (2021). Green synthesis of magnetic nanoparticles using satureja hortensis essential Oil toward superior antibacterial/Fungal and anticancer performance. *BioMed Research International*, 2021(9), 1–14. DOI 10.1155/2021/8822645.
6. Tyagi, V. V., Kaushik, S. C., Tyagi, S. K., Akiyama, T. (2011). Development of phase change materials based microencapsulated technology for buildings: A review. *Renewable & Sustainable Energy Reviews*, 15(2), 1373–1391. DOI 10.1016/j.rser.2010.10.006.
7. Zhang, Z. L., Li, L. J., Sun, D., Wang, M., Shi, J. R. et al. (2020). Preparation and properties of chitosan-based microspheres by spray drying. *Food Science & Nutrition*, 8(4), 1933–1941. DOI 10.1002/fsn3.1479.

8. Liu, J. Y., Liu, C. H., Liu, Y. J., Chen, M. J., Hu, Y. et al. (2013). Study on the grafting of chitosan-gelatin microcapsules onto cotton fabrics and its antibacterial effect. *Colloids and Surfaces B: Biointerfaces*, 109, 103–108. DOI 10.1016/j.colsurfb.2013.03.040.
9. Wang, X. Y., Heuzey, M. C. (2016). Pickering emulsion gels based on insoluble chitosan/gelatin electrostatic complexes. *RSC Advances*, 6(92), 89776–89784. DOI 10.1039/C6RA10378B.
10. Bajpai, V. K., Sharma, A., Baek, K. H. (2015). Antibacterial mode of action of *Ginkgo biloba* leaf essential oil: Effect on morphology and membrane permeability. *Bangladesh Journal of Pharmacology*, 10(2), 337–350. DOI 10.3329/bjp.v10i2.22546.
11. Bajpai, V. K., Kim, Y., Baek, K. H. (2017). Phenolic content, lipid peroxidation inhibition and antioxidant potential of leaf essential oil of *Ginkgo biloba* in various scavenging models. *National Academy Science Letters*, 40(2), 95–99. DOI 10.1007/s40009-016-0530-5.
12. Yang, D., Wang, X. Y., Gan, L. J., Zhang, H., Shin, J. A. et al. (2015). Effects of flavonoid glycosides obtained from a *Ginkgo biloba* extract fraction on the physical and oxidative stabilities of oil-in-water emulsions prepared from a stripped structured lipid with a low omega-6 to omega-3 ratio. *Food Chemistry*, 174, 124–131. DOI 10.1016/j.foodchem.2014.11.036.
13. Niu, X., Liu, Y., Song, Y., Han, J. Q., Pan, H. (2018). Rosin modified cellulose nanofiber as a reinforcing and co-antimicrobial agents in polylactic acid/chitosan composite film for food packaging. *Carbohydrate Polymers*, 183, 102–109. DOI 10.1016/j.carbpol.2017.11.079.
14. Monika, Dhar, P., Katiyar, V. (2017). Thermal degradation kinetics of polylactic acid/acid fabricated cellulose nanocrystal based bionanocomposites. *International Journal of Biological Macromolecules*, 104, 827–836. DOI 10.1016/j.ijbiomac.2017.06.039.
15. Chang, S. H., Chen, Y. J., Tseng, H. J., Hsiao, H. I., Chai, H. J. et al. (2021). Antibacterial activity of chitosan-poly lactate fabricated plastic film and its application on the preservation of fish fillet. *Polymers*, 13(5), 696. DOI 10.3390/polym13050696.
16. Yadav, J. P., Kumar, S., Budhwar, L., Yadav, A., Yadav, M. (2016). Characterization and antibacterial activity of synthesized silver and iron nanoparticles using *Aloe vera*. *Journal of Nanomedicine & Nanotechnology*, 7(3), 384. DOI 10.4172/2157-7439.1000384.
17. Ahmed, S., Saif, U., Ahmad, M., Swami, B. L., Ikram, S. (2016). Green synthesis of silver nanoparticles using *Azadirachta indica* aqueous leaf extract. *Journal of Radiation Research and Applied Sciences*, 9(1), 1–7. DOI 10.1016/j.jrras.2015.06.006.
18. Nguyen, N. T. H., Nguyen, L. V. H., Thanh, N. T., Toi, T. N., Quyen, T. N. et al. (2019). Stabilization of silver nanoparticles in chitosan and gelatin hydrogel and its applications. *Materials Letters*, 248, 241–245. DOI 10.1016/j.matlet.2019.03.103.
19. Geng, X. Y., Li, W., Yin, Q., Wang, Y., Han, N. et al. (2018). Design and fabrication of reversible thermochromic microencapsulated phase change materials for thermal energy storage and its antibacterial activity. *Energy*, 159, 857–869. DOI 10.1016/j.energy.2018.06.218.
20. Tomke, P. D., Rathod, V. K. (2020). Facile fabrication of silver on magnetic nanocomposite ($\text{Fe}_3\text{O}_4@$ chitosan–AgNP nanocomposite) for catalytic reduction of anthropogenic pollutant and agricultural pathogens. *International Journal of Biological Macromolecules*, 149, 989–999. DOI 10.1016/j.ijbiomac.2020.01.183.
21. Jiang, J. Y., Gong, L., Dong, Q. F., Kang, Y. F., Osako, K. et al. (2020). Characterization of PLA-p3, 4HB active film incorporated with essential oil: Application in peach preservation. *Food Chemistry*, 313, 126134. DOI 10.1016/j.foodchem.2019.126134.
22. Yang, C. X., Tang, H. B., Wang, Y. F., Liu, Y., Wang, J. et al. (2019). Development of PLA-PBSA based biodegradable active film and its application to salmon slices. *Food Packaging and Shelf Life*, 22, 100393–100393. DOI 10.1016/j.fpsl.2019.100393.
23. Yuan, M. X., Ning, C., Yang, S. X., Liang, Q. P., Mou, H. J. et al. (2020). A new cold-active glucose oxidase from penicillium: High-level expression and application in fish preservation. *Frontiers in Microbiology*, 11, 606007. DOI 10.3389/fmicb.2020.606007.

24. Mi, H. B., Zhao, B., Wang, C., Yi, S. M., Xu, Y. X. et al. (2017). Effect of 6-gingerol on physicochemical properties of grass carp (*Ctenopharyngodon idellus*) surimi fortified with perilla oil during refrigerated storage. *Journal of the Science of Food and Agriculture*, 97(14), 4807–4814. DOI 10.1002/jsfa.8350.
25. Wu, Y. Z., Wang, J. C., Song, S. Q., Rao, P. H., Wang, R. K. et al. (2020). Biochemical changes and amino acid deamination & decarboxylation activities of spoilage microbiota in chill-stored grass carp (*Ctenopharyngodon idella*) fillets. *International Journal of Biological Macromolecules*, 336, 127683. DOI 10.1016/j.foodchem.2020.127683.
26. Singhal, G., Bhavesh, R., Kasariya, K., Sharma, A. R., Singh, R. P. (2011). Biosynthesis of silver nanoparticles using *Ocimum sanctum* (Tulsi) leaf extract and screening its antimicrobial activity. *Journal of Nanoparticle Research*, 13(7), 2981–2988. DOI 10.1007/s11051-010-0193-y.
27. Vidhu, V. K., Aromal, S. A., Philip, D. (2011). Green synthesis of silver nanoparticles using *Macrotyloma uniflorum*. *Spectrochimica Acta Part A: Molecular and Biomolecular Spectroscopy*, 83(1), 392–397. DOI 10.1016/j.saa.2011.08.051.
28. Kumar, B., Angulo, Y., Smita, K., Cumbal, L., Debut, A. (2016). Capuli cherry-mediated green synthesis of silver nanoparticles under white solar and blue LED light. *Particuology*, 24(1), 123–128. DOI 10.1016/j.partic.2015.05.005.
29. Vorobyev, S., Vishnyakova, E., Likhatski, M., Romanchenko, A., Nemtsev, I. et al. (2019). Reactivity and chemical sintering of carey lea silver nanoparticles. *Nanomaterials*, 9(11), 1525. DOI 10.3390/nano9111525.
30. Wang, J. L., Zhan, L. L., Zhang, X. H., Wu, R. F., Liao, L. et al. (2020). Silver nanoparticles coated poly(L-lactide) electrospun membrane for implant associated infections prevention. *Frontiers in Pharmacology*, 11, 431. DOI 10.3389/fphar.2020.00431.
31. Ambroziak, R., Holdynski, M., Plocinski, T., Pisarek, M., Kudelski, A. (2019). Cubic silver nanoparticles fixed on TiO₂ nanotubes as simple and efficient substrates for surface enhanced Raman scattering. *Materials*, 12(20), 3373. DOI 10.3390/ma12203373.
32. Wu, Y. Z., Wang, J. C., Song, S. Q., Rao, P. H., Wang, R. K. et al. (2020). Preparation and application properties of sustainable gelatin/chitosan soil conditioner microspheres. *International Journal of Biological Macromolecules*, 159(2), 685–695. DOI 10.1016/j.ijbiomac.2020.05.122.
33. Yousefi, M., Khorshidian, N., Mortazavian, A. M., Khosravi-Darani, K. (2019). Preparation optimization and characterization of chitosan-tripolyphosphate microcapsules for the encapsulation of herbal galactagogue extract. *International Journal of Biological Macromolecules*, 140, 920–928. DOI 10.1016/j.ijbiomac.2019.08.122.
34. Roy, J. C., Giraud, S., Ferri, A., Mossotti, R., Guan, J. P. et al. (2018). Influence of process parameters on microcapsule formation from chitosan-type B gelatin complex coacervates. *Carbohydrate Polymers*, 198, 281–293. DOI 10.1016/j.carbpol.2018.06.087.
35. Geethalakshmi, R., Sarada, D. V. L. (2012). Gold and silver nanoparticles from *Trianthema decandra*: Synthesis, characterization, and antimicrobial properties. *International Journal of Nanomedicine*, 7, 5375–5384. DOI 10.2147/IJN.
36. Han, Y., Gao, Y., Cao, X. Q., Zangeneh, M. M., Liu, S. K. et al. (2020). Ag NPs on chitosan-alginate coated magnetite for synthesis of indazole 2, 1-b phthalazines and human lung protective effects against α -guttiferin. *International Journal of Biological Macromolecules*, 164, 2974–2986. DOI 10.1016/j.ijbiomac.2020.08.183.
37. Matica, M. A., Aachmann, F. L., Tondervik, A., Sletta, H., Ostafe, V. (2019). Chitosan as a wound dressing starting material: Antimicrobial properties and mode of action. *International Journal of Molecular Sciences*, 20(23), 5889. DOI 10.3390/ijms20235889.
38. Shankar, S., Rhim, J. W., Won, K. (2018). Preparation of poly(lactide)/lignin/silver nanoparticles composite films with UV light barrier and antibacterial properties. *International Journal of Biological Macromolecules*, 107, 1724–1731. DOI 10.1016/j.ijbiomac.2017.10.038.
39. Ali, S., Chen, X. J., Shah, M. A., Ali, M., Zareef, M. et al. (2021). The avenue of fruit wastes to worth for synthesis of silver and gold nanoparticles and their antimicrobial application against foodborne pathogens: A review. *Food Chemistry*, 359(35), 129912. DOI 10.1016/j.foodchem.2021.129912.

40. Huang, L. Y., Dai, T. H., Xuan, Y., Tegos, G. P., Hamblin, M. R. (2011). Synergistic combination of chitosan acetate with nanoparticle silver as a topical antimicrobial: Efficacy against bacterial burn infections. *Antimicrobial Agents and Chemotherapy*, 55(7), 3432–3438. DOI 10.1128/AAC.01803-10.
41. Qin, N., Li, D. P., Hong, H., Zhang, Y. M., Zhu, B. W. et al. (2016). Effects of different stunning methods on the flesh quality of grass carp (*Ctenopharyngodon idellus*) fillets stored at 4°C. *Food Chemistry*, 201, 131–138. DOI 10.1016/j.foodchem.2016.01.071.
42. Zhang, J. B., Li, Y., Liu, X. C., Lei, Y. T., Regenstein, J. M. et al. (2019). Characterization of the microbial composition and quality of lightly salted grass carp (*Ctenopharyngodon idellus*) fillets with vacuum or modified atmosphere packaging. *International Journal of Food Microbiology*, 293, 87–93. DOI 10.1016/j.ijfoodmicro.2018.12.022.
43. Zhu, Z. W., Gao, H., Gao, T. T., Sun, D. W. (2018). Quality comparison of grass carp and salmon fillets packaged in modified atmosphere with different composite films. *Journal of Food Process Engineering*, 41(5), e12803. DOI 10.1111/jfpe.12803.